Nanoscale

Accepted Manuscript

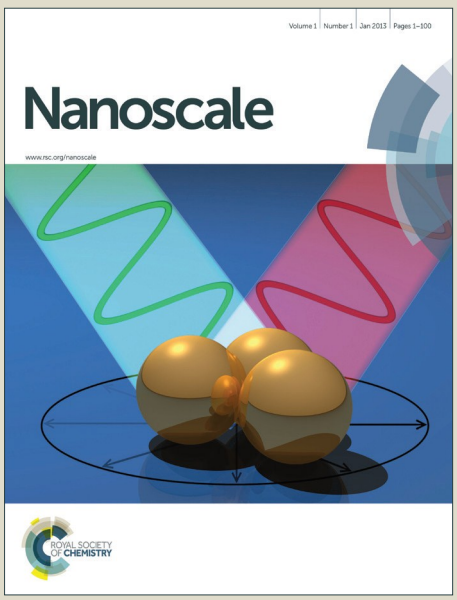

ROYAL SOCIETY OF CHEMISTRY

www.rsc.org/nanoscale

Plasmonic Fluorescent CdSe/Cu_2S Hybrid Nanocrystals for Multichannel Imaging and Cancer Directed Photo-Thermal Therapy

M. Sheikh Mohamed [1+], Aby Cheruvathoor Poulose [1+], Srivani Veeranarayanan [1], Rebeca Romero Abeurto [2], Trevor Mitcham [3], Yuko Suzuki [4], Yasushi Sakamoto [4], Pulickel M. Ajayan [2], Richard R. Bouchard [3], Yasuhiko Yoshida [1], Toru Maekawa [1], D. Sakthi Kumar [1*]

[1]*Bio-Nano Electronics Research Center, Toyo University, 2100, Kujirai, Kawagoe, Saitama, Japan- 350-8585*

[2]*Department of Material Science and NanoEngineering, Rice University, 6100 Main Street, Houston, TX 77005, USA*

[3]*Department of Imaging Physics, University of Texas MD Anderson Cancer Center, Houston, TX 77054, USA*

[4]*Biomedical Research Centre, Division of Analytical Science, Saitama Medical University, Saitama 350-0495, Japan*

Authors Contributed Equally to this Work[+]

Corresponding author*
Prof. D. Sakthi Kumar,
Ph: 81-492-39-1636
Fax: 81-492-34-2502
E-mail: sakthi@toyo.jp

Abstract:

A simple, crude Jatropha curcas (JC) oil-based synthesis approach, devoid of any toxic phosphine and pyrophoric ligands, to produce size and shape tuned CdSe QDs and a further copper sulfide (Cu_2S) encasing is presented. The QDs exhibited excellent photoluminescent properties with narrow band gap emission. Furthermore, the Cu_2S shell rendered additional cytocompatibility and stability to the hybrid nanomaterial, which are major factors for translational and clinical applications of QDs. The nanocomposites were PEGylated and folate conjugated to augment their cytoamiability and enhance specificity towards cancer cells. The nanohybrids possessed visible, near infrared (NIR), photoacoustic (PA) and computed tomography (μCT) imaging potentials. The diverse functionality of the composite was derived from the multi-channel imaging abilities and thermal competence on NIR laser irradiation to specifically actuate photo-thermal ablation of brain cancer cells.

Keywords: Quantum Dots, Jatropha Curcas, Cancer, Photo-thermal therapy, Imaging.

Introduction:

With nanotechnology at its prime and applications as diverse as electronics, engineering to biomedicine, the core objective of researchers has been to device easy and scalable strategies for the production of high quality and performance nanomaterials.[1-6] The efficiency of any nanomaterial depends finally upon its application and performance. One field where nanomaterials are rapidly expanding in application is nanomedicine for cancer therapy and the like, which has the potential to overcome currently faced challenges by enabling the engineered nanoformulations to discretely navigate the body and perform functions in very controlled and specific ways.[7,8] Current focus is on combining multiple components, with distinct characteristics, into a single multifunctional nanocomposite to impart diversified therapeutic and diagnostic features. Most of such nanocomposites consist of an imaging probe, as QDs or fluorescing molecules, and a carrier system, as silica, poly ethylene glycol (PEG) or noble metals.[9-12] These composite or hybrid nanomaterials are expected to perform signature activities unique to individual components of the system or as a complex unit working in synergy.[13,14] Such a typical hybrid nanomaterial would be capable of carrying one or multiple drug payloads, dye or quantum nanocrystals (NCs) for imaging in addition to the presence of inherent capabilities of the carrier system as magnetic-, near infrared (NIR)-, surface enhanced raman spectrum (SERS)-, ultrasound-, photoacoustic-responsiveness etc.[15-19] These multiple functionalities could provide additional diversified imaging options as visible fluorescence imaging, magnetic resonance imaging (MRI), NIR imaging, photo-acoustic and ultrasound imaging etc, and a combination of treatment options as chemotherapeutic, photo-thermal therapy, hyperthermia etc.[20-23]

One particular hurdle in combining fluorophores such as semiconductor quantum dots with plasmonic materials is the issue of drastic fluorescence quenching.[24,25] So far, the combination of quantum dot fluorescence with plasmonically active gold has only been demonstrated on flat surfaces.[26] One resolve regarding this issue was the bridging of pre-formed QDs and gold nanoparticles with nanometer length peptides for biosensing,[27] which decreased the fluorescence quenching to a commendable extent. Despite these recent advances, a prolonging hurdle exists in functionalizing QDs with plasmonic materials while still maintaining the unique electronic and optical properties of both nanocomponents to a significant level. In this context, the amalgamation of plasmonic nanostructures with luminescent quantum dots to form core–shell composites has great potential for simultaneous multimodal bioimaging and hyperthermal therapy.

Herein, we report a simple and relatively innocuous synthesis process of high quality CdSe QDs using crude *Jatropha curcas* oil as capping cum co-ordinating reagent. The oil was extracted from *J. curcas* seeds by a one step ether extraction. In addition, the development of metal sulfide (Cu_2S)-encapsulated CdSe QDs, also employing the same oil, with well-defined and preserved optical properties was elucidated. The CdSe/Cu_2S QDs were PEGylated and folate conjugated to impart additional biocompatibility and cancer targeting potential. In addition, the NIR-absorbance mediated by plasmonically active shell assisted in NIR and photoacoustic imaging, whereas the X-ray attenuation ability of core material, Cd, served as X-ray contrast agent. The nanocomposites were tested and proven for their CdSe/Cu_2S based imaging and Cu_2S derived photo-thermal ablation properties against normal and brain cancer cells.

Materials and Methods:

Materials:

Dulbecco's modified eagle's medium (DMEM), phosphate buffered saline (PBS) (pH 7.2) and live/dead double staining kit were purchased from Sigma-Aldrich. 0.25% Trypsin, antibiotics (Penicillin, Streptomycin) and Fetal bovine serum (FBS) were from Gibco. Alamar Blue and NucBlue Live (Hoechst) were from Invitrogen. DSPE-PEG-COOH {1,2-distearoyl-*sn*-glycero-3-phosphoethanolamine-N-[carboxy (polyethylene glycol)-2000] (ammonium salt)} and DSPE-PEG-FOL {1,2-distearoyl-*sn*-glycero-3-phosphoethanolamine-N-[folate (polyethylene glycol)-2000] (ammonium salt)} were purchased from Avanti polar lipids. All other chemicals and reagents were of analytical grade acquired from either Sigma-Aldrich or Wako chemicals.

Extraction of crude JC Oil:

Jatropha curcas crude oil was extracted from 150 g of de-shelled mature seeds in a waring blender with 1.5 L of cold diethyl ether. The slurry was centrifuged at 12,000 rpm at 4 °C and the supernatant collected in a beaker. The supernatant was allowed to air dry in a fume hood, for the complete evaporation of ether. After one week, all the ether had evaporated leaving behind the crude oil. The oil was centrifuged to sediment any remnants of seed debris, and the supernatant oil was designated as crude JC oil and used in further synthesis process without any modifications.

Synthesis of CdSe QDs:

Typically, Se precursor solution was obtained by dissolving 0.0078 g (0.1 mmol) of Se in 1 mL of JC oil at 250 °C for 30 min. The solution was then cooled down to

room temperature. Meanwhile, a mixture of CdO powder (0.1 mmol), JC oil (5 mL) and octadecene (10 mL) was stirred in a three-neck flask. This mixture was heated to 300 °C under Ar flow till the solution became transparent indicating the complete dissolution of CdO in the oil. Subsequently, the Se solution was swiftly injected into the vigorously stirred reaction flask. After the injection, the temperature was kept for 2 min at 300 °C for the growth of CdSe NCs, then immediately cooled down to room temperature. The NCs were precipitated with ethanol by centrifuging at 9000 rpm for 5 min, washed thrice and dispersed in chloroform.

Synthesis of CdSe/Cu_2S NCs:

Copper precursor solution was obtained by dissolving 0.1 mmol of Cu (I) Cl in 1 mL of JC oil and 4 mL of octadecene. The solution was heated to 110 °C for 30 min to dissolve Cu salt. Sulfur solution was prepared by adding 0.1 mmol of S to 1 mL of JC oil and the mixture was heated to 200 °C for 30 min. To prepare core-shell NCs, 1 mL of as prepared CdSe QDs dispersed in octadecene was added to a three-neck flask and heated to 180 °C. Once the temperature reaches 180 °C, 1 mL of Cu solution and 100 μL of S solution were added. The reaction was proceeded for 30 min at 180 °C and immediately cooled down to room temperature. Excess amount of ethanol was used to precipitate the core-shell NCs by centrifuging at 9000 rpm for 5 min, washed repeatedly and finally dispersed in chloroform.

MPA coated CdSe and CdSe/Cu_2S NCs:

To 1 mg/mL of NC solution in chloroform, 1 mL of 0.1 M MPA solution (MPA in methanol, pH 10) was added. The solution was mixed by gentle shaking after which 1 mL of de-ionized H_2O was added. Ligand exchange occurs by the replacement of JC

oil capping by MPA. The upper aqueous phase distributed NCs were carefully removed by pipetting and pelleted by centrifugation. The final product was re-dispersed in 1 mL of de-ionized H_2O.

DSPE-PEG coated CdSe and CdSe/Cu_2S NCs:

The NCs were DSPE-PEG coated by thin film hydration. 1 mg/mL of chloroform dispersed NCs (non-MPA coated) were mixed with solution of 1 mg/mL DSPE-PEG-COOH (dispersed in chloroform and methanol in the ration of 20:1). The NCs-DSPE-PEG mixture was desiccated overnight to form a thin film. The film was hydrated with PBS buffer (pH 7) and sonicated for 15 min to prepare water dispersible DSPE-PEG coated NCs. For imparting targeting ability to CdSe/Cu_2S NCs (PF-CdSe/Cu_2S), 100 μg/mL DSPE-PEG-Fol was utilized along with DSPE-PEG-COOH (1:10 M ratio) and the process was similar as above.

JC Oil and particle characterization techniques:

To analyze the rough composition of the crude JC oil, NMR (JEOL 400 mHz) was performed. The morphology and Energy Dispersive X-ray Spectroscopy (EDS) of as prepared CdSe QDs and CdSe/Cu_2S NCs were analyzed with the help of field emission transmission electron microscope (TEM), (JEOL JEM-2200-FS). For the TEM analysis of CdSe, the QDs were drop-casted on a 200 mesh Cu microgrid (with film) whereas for CdSe/Cu_2S NCs a 200 mesh Ni grid (with film) was used. Fourier transform infrared spectroscopy (FT-IR ATR crystal Spectrometer, Thermo Scientific) analysis was performed to investigate the chemical bonding characteristics of JC oil and NPs. UV-Vis spectrophotometry (Shimadzu UV-2100PC/3100PC UV visible spectrometer) was performed to determine the plasmonic properties of the NPs.

Photoluminescence (PL) spectra were recorded using a JASCO FP 6500 spectrofluorometer at an excitation wavelength of 365 nm. Zeta potential of the NCs were measured by Malvern Zetasizer Nano-ZS.

Mouse phantom imaging:

The CdSe/Cu_2S NCs, at a concentration of 5 mg/mL were filled in a silicon tube and imaged in a ClairVivo Opt In vivo imaging system (Shimadzu, Japan) using Cy 7 filter (excitation wavelength: 650 nm and emission wavelength: 810 nm) with an exposure time of 60 seconds. The NCs filled tube was then inserted in the rear cavity of the mouse phantom in a diagonal position to image the presence of the NCs at various depths in the phantom.

Photoacoustic imaging:

VisualSonics Vevo LAZR- 2100 high-frequency photoacoustic system was employed to assess the PA imaging potential of the hybrid NCs. PEGylated CdSe/Cu_2S NCs were injected into a vinyl tubing which does not generate a significant PA signal, therefore negating major interference signals from the tubing itself. The NCs filled tubes were sealed at the ends with epoxy and suspended in a container filled with a mixture of water and milk (2% fat by volume), added for optical scattering. The sample was imaged with a 21 MHz linear array from 680 to 970 nm with a step size of 2 mm to determine the peak signal produced by the NCs.

X-Ray µCT contrast imaging:

The μCT contrast potential of CdSe/Cu_2S NCs was analyzed at 45 KeV tube voltage using a μCT system (ScanCo, Switzerland). The NCs were partially dried and were loaded onto filter paper strips before placing inside the phantom tubes for analysis.

Cell culture maintenance:

Glioma (human brain glioblastoma) and HCN-1A (human cortical neurons) cell lines were acquired from Riken Bioresources, Japan and ATCC respectively, and maintained in T25 flasks using DMEM medium supplemented with 10% FBS and antibiotics in an incubator at 37 °C with 5 % CO_2. The cells were sub-cultured every 2 days. Cells were cultured on glass base dishes for confocal microscopy studies and in 96 well plates for cytotoxicity studies.

Cell based assays:

Cytotoxicity was assayed with the help of alamar blue. The principle of the assay involves the conversion of non-fluorescent alamar blue into a fluorescent moiety, whose absorbance could be read at 560 nm, by metabolically active cells and is not possible with cells undergoing death. Post confluency, Glioma and HCN-1A were trypsinized, pelleted and approximately 5000 cells added to each well of 96 well plates and cultured for 24 h prior to NCs exposure. All experiments were conducted in triplicates. Controls were maintained devoid of any treatment, whereas test groups were treated with 100 μL (1 mg/mL, 0.1 mg/mL and 0.01 mg/mL) of respective NCs. The plates were incubated for 48 h after which the fluorescence intensity of the final product was analyzed with a microplate spectrofluorimeter (Multidetection microplate scanner, Dainippon Sumitomo Pharma). The viable percentage of cells were calculated for each group and plotted against concentration of NCs. For analysis of

cellular internalization of the NCs, approximately 25,000 cells were plated onto 35 mm glass base dishes for 24 h. 100 µL of 0.1 mg/mL NCs were added to the plates and incubated for 2 h at culture conditions followed by 20 min incubation with Nuc blue. After the incubation period, cells were washed thoroughly and analyzed under an excitation wavelength of 561 nm (for NCs) and 405 nm (for Hoechst) under a high-speed confocal laser-scanning microscope (CLSM, Olympus IX 81 under DU897 mode) to visualize particle uptake. Next to quantitatively estimate particle uptake, cells (90 % confluence in T25 flask) exposed to 1 mg/mL of NCs were collected and microwave digested using HNO_3. Post digestion, the atomic percentage of Cu, Cd and Se were estimated using ICP-MS (iCAP Q, Thermofisher Scientific).

Photothermal studies:

A highly monochromatic, collimated beam of NIR range (800 nm) [Chameleon Ultra diode-Pumped Mode Locked-Sub 200 Femtosecond Laser (Coherent 80 MHz repetition rate)] with power 2.027 W/cm^2 (Laser power meter: VEGA, OPHIR, Japan) was utilized. The temperature variations were measured and analyzed with an infra-red (IR) thermometer [Thermal imager test 881-2 (Testo AG, Germany)]. To determine the concentration dependent photothermal responsiveness of CdSe/Cu_2S NCs, different concentrations of toluene dispersed NCs were irradiated with NIR laser of wavelength and power as above. To further investigate the photothermal conversion efficiency of the NCs, we recorded the temperature change of the sample (100 µg/mL) as a function of time under NIR laser for 600 s.

For photothermal ablation of cells, approximately 25,000 cells were grown in glass base dishes. The cells were treated with CdSe/Cu_2S and PF-CdSe/Cu_2S NCs (0.1 mg/mL) and subjected to NIR laser exposure for 4 min, after which they were stained

using Calcein/PI live/dead staining kit. All the experiments were conducted in triplicates and the cells were thoroughly washed to remove unbound NPs and stains prior to analysis.

Results and Discussion:

Cadmium chalcogenide CdSe QDs were prepared by simple plant oil mediated synthesis route. Conventional chemicals have formed the backbone of nanomaterial synthesis for a long time. It has to be reckoned with though, that these chemicals are seldom environmentally compatible and also do not fit the cost-effective criterion. There have been initiatives to synthesize nanomaterials, especially metal nanoparticles, from alternative sources that have yielded commendable success. [28-30] However, certain classes of nanoparticles (NPs), especially semiconductor NPs require, by default, the use of chemicals which facilitate the coordination and stability of the NPs especially phosphine based chemicals,[31-34] which apart from being expensive, are also highly noxious to the environment.[35-37] This too was overcome to an extent, by using vegetable oils, which negated the use of phosphines, to synthesize high quality NPs.[38-40] Despite such a beneficial role, the major drawback was that such oils (as olive oil etc.) belong to the edible oil category.

Jatropha curcas or physic nut has been known as the 'wonder crop' with seed oil content of upto 50 %.[41] It has become synonymous with its claim of being an alternative fuel (biodiesel) crop. [42-44] The major fatty acid components of the seed oil are oleic acid (34.3-45.8%), linoleic acid (29.0-44.2%), palmitic acid (14.1-15.3%) and stearic acid (3.7-9.8%).[45] It has been well established that oleic acid (OA) plays a vital role in semiconductor nanocrystal stabilization during synthesis. [46-49] The high OA content of the *J. curcas* oil along with its high boiling point are ideal for use as a

solvent and stabilizing agent in nanomaterial synthesis. The fact that JC oil is non-edible, renewable, non-competent to food crops and of industrial grade, aptly supplements its claim for such a consideration.

Oil mediated hot injection synthetic route was considered to be advantageous for several reasons compared to conventional oleic acid-trioctyl phosphine (TOP) based synthesis: a) toxic phosphine free synthetic method, b) *Jatropha* oil itself can act as both capping and coordinating agent, c) low cost, d) cleaner methodology and e) easily scalable for mass production of QDs. The choice of *Jatropha* oil was justified by NMR analysis (Fig. S1), with sharp peaks referencing the presence of signature fatty acids and triglycerides (Fig. S1 inset). Though the extraction process was relatively simpler and the oil was termed as 'crude', still it had high level of resemblance to the conventionally extracted pure oils.[50,51] The oil is composed mainly of oleic and linoleic acids along with triglyceride esters. It was attempted to utilize this composition as a capping and stabilizing ligand for governing the quality of CdSe QDs including size, size distribution, and crystallinity and subsequent coating with Cu_2S shell.

Morphological evaluation of the CdSe QDs by TEM revealed particles of uniform size (3-5 nm) with high level of monodispersity (Fig. 1a). The high-resolution TEM images of CdSe QDs showed sharp crystal lattice patterns with the interplane-distance of (220) crystal planes being 3.5 Å (Fig. 1b), corresponding to the standard cubic CdSe phase (JCPDS no. 65-2891). EDS spectra of the QDs (Fig. S2a) confirmed the presence of Cd and Se without any impurities (Atomic % of Cd-42.51 and Se-57.49 %). In the case of CdSe/Cu_2S NCs (13-17 nm), it was observed that all QDs were completely coated with a Cu_2S shell, though the thickness of the shell varied (Fig. 1d). The high magnification HRTEM image showed closely packed lattice structure

with an interplane distance of 1.96 Å (110) depicting the formation of Cu_2S Digenite (JCPDS no. 47-1748) and a core-shell hybrid nanostructure that demarcated metal sulfide coating on the core QD (Fig. 1e). In addition, EDS (Fig. S2b) and XPS (Fig. S3) revealed the presence of Cu and S along with Cd and Se. The atomic percentages of Cu, S, Cd and Se were found to be 35.81, 20.19, 20.52 and 23.48 respectively with the help of EDS analysis. The XRD pattern matches well with the Zinc Blend (cubic) CdSe (JCPDS 65-2891) and Digenite (Rhombohedral Hexagonal) Cu_2S (JCPDS 47-1748) structure further confirmed the purity of the as synthesized core-shell nanostructures (Fig. S4).

It is well known that *Jatropha* oil is rich in fatty acids. Oleic acid and Linoleic acid were found in abundance and make up for 80 % of fatty acid content making them an ideal capping cum co-ordinating solvent for synthesis of various NCs. The FT-IR analysis (Fig. 2) of JC oil, as such was performed to elucidate the possible mechanism in functioning as an efficient, alternative stabilizing medium. The oil presented signature peaks at 690 cm^{-1} (CH_2 bend), 1125 cm^{-1} (C-O stretch), 1375 cm^{-1} (CH_3 bend), 1446 cm^{-1} (CH_2 in plane bend), 1750 cm^{-1} (C=O stretch) and 2853, 2924 cm^{-1} (C-H stretch).[52] These prominent peaks relate to the fatty acids in the oil. In addition, post heating the oil to 300 °C, to assess the changes/degradation if any at the high reaction temperatures, it was observed that all of the above mentioned bonds were retained, confirming that JC oil can withstand high temperatures without any thermochemical degradation, a pre-requisite for solvents in high quality NC synthesis. The CdSe QDs and CdSe/Cu_2S NCs also exhibited all the characteristic peaks of the oil. However, it was noticed that C-O stretch peak centered at 1125 cm^{-1} was comparatively weaker. It is well known, that O-H of carboxylic acids (present in oleic/fatty acids) are responsible for capping the NCs.[53] The interaction of O-H with

NCs surface, i.e., with Cd/Cu, causes the weakening of C-O stretch. Thus C-O stretch vibration becomes feeble and a weaker signal emanates from the oil capped NCs supporting the major involvement of JC oil as a proper capping agent aiding in nucleation and stabilization of NCs.

As one would expect, coating of metals onto QDs would drastically quench their luminescence. This significant drawback limits the synthesis of many multifunctional structures based on QDs and metal NPs. To elucidate the effect of Cu_2S coating in the present scenario, we analyzed the photophysical nature of bare CdSe and core-shell CdSe-Cu_2S NCs. The absorbance spectra (Fig. 3a) clearly indicated that CdSe QDs as such exhibited absorbance at 550 – 600 nm whereas the core-shell exhibited 2 absorption peaks, one at 550 – 600 nm, corresponding to the absorbance of core QD and the other broad absorption at NIR region, corresponding to the localized surface plasmon resonance (LSPR) of copper sulfide.[54] The dual absorbance referred to the presence of hybrid structures. When the photoluminescence of bare and core-shell structure was investigated (Fig. 3b), the QDs exhibited a narrow emission peak centered at 590 nm whereas the CdSe/Cu_2S structure exhibited a broader emission spanning from 400 – 850 nm. This broad emission was split into two major discrete peaks centered at 520 nm and 625 nm. The emission at 520 nm possibly suggests that during core-shell NC preparation, the core material could be etched/replaced by Cu_2S leading to reduction/maintenance of size thereby blue-shifting the emission, whereas the emission at 625 nm may be due to the formation of CdSeS hybrid interface which may shift the band edge of QDs. Also, the broad NIR emission could be due to the Cu_2S in the heterostructures. The PL spectra suggest the reduction but retention of significant level of fluorescence of the CdSe QDs post heterostructure formation. The observed quenching may be related to the possible electron transfer from CdSe to

Cu_2S, thereby restricting or reducing the radiative recombination from conduction band to valence band of CdSe QDs. Additionally, the band gap of bare CdSe and core-shell CdSe/Cu_2S was calculated using Tauc equation and found to be 2.04 eV and 2.06 eV respectively.

The PL observations revealed a curious possibility of the hybrid nanomaterial to be used in NIR imaging, based on its broad emission spectra. The NCs were filled in a silicon tube and imaged as such to confirm this speculation. The empty silicon tube was also imaged to observe any autofluorescence interference from the tube itself. It could be clearly visualized that the NC filled tube presented higher fluorescence intensity under the Cy 7 filter at the regions where the NCs had been concentrated (Fig. 4b left inset). The empty tube and the part of tube devoid of NCs did not reveal any fluorescence. The same was investigated in a mouse phantom, mimicking to a great extent the morphology and thickness of a live mouse (Fig. 4a). As could be seen from fig 4b, the fluorescence from the NCs was recorded from inside the phantom spanning various depths. This assessment could in principle be translated to the usefulness of the CdSe/Cu_2S hybrids in *in vivo* NIR imaging.

The multi channel-imaging claim of the NCs was put to test by analyzing their photo acoustic (PA) signal amplitudes. The particles appeared well responsive under PA imaging and followed the expected spectrum more or less until the energy of the Vevo plummeted around 930 nm. It is really difficult to get reliable data past that point as the light fluence is simply too low to generate a reliable signal from anything but a wire in a water bath. The spectroscopic imaging of NCs generated a PA signal spectrum that peaked around 900 nm. Moreover, the broad absorption of the NCs opens up the possibility of using cost-effective laser sources for PA imaging. In addition, the NCs showed exceptionally broad spectral response (Figure. 5a). When

evaluated at a preclinical frequency (21 MHz), the NCs could be nicely visualized with PA imaging system (Figure. 5c), however produced poor signal with ultrasound alone (Figure. 5b).

Additionally, the CdSe/Cu_2S NCs were investigated for their X-ray attenuation based contrast responsiveness. Micro computed tomography (μCT) imaging, is a widely accepted and utilized contrast imaging modality in medical diagnostics owing to its deep tissue penetration and high resolution characteristics. Figure 6 represents the X-ray CT image of CdSe/Cu_2S NCs and their cross-sectional Z-stacked images portraying significantly enhanced signals, demonstrating the prospective application of these hybrid NCs as CT contrast agents.

As the multi-imaging potential of the NCs was affirmed, the functionality of the Cu_2S shell as such was investigated. Cu based chalcogenides are known to exhibit LSPR facilitating their ability to generate heat upon NIR laser exposure.[55,56] CdSe-Cu_2S NCs dispersed in PBS were subjected to NIR laser exposure (800 nm) for a period of 2 min. It could be noted from the thermal mapping (Fig. S7) that the temperature rose to 60 °C within the time period of exposure. Also, a concentration dependent rise in temperature was observed (Fig. 7a). As CdSe QDs do not possess the intrinsic ability to excite upon NIR laser irradiation, and water as such cannot do the same, the temperature rise was attributed to the Cu_2S shell, indirectly evidencing the presence of proper coating in the heterostructure. The photothermal conversion efficiency of CdSe/Cu_2S NCs was calculated to be ~11.65%.[57]

We further investigated the *in vitro* applicability of the CdSe and CdSe/Cu_2S as visible imaging and photothermal candidates, respectively. Since the as-prepared NPs were hydrophobic due to their JC oil capping, a phase-transfer using MPA was performed. MPA coated CdSe and CdSe/Cu_2S NCs were water-dispersed and

analyzed for their cytocompatibility towards normal cortical neurons and cancerous brain glioblastoma cell lines. As shown in figure 8a MPA-coated CdSe QDs at a concentration of up to 0.1 mg/mL did not affect the cell viability of both the cell lines under study until 72 h of incubation, though a slight reduction in viability was observed at a concentration of 1 mg/mL. This could be attributed to leaching of Cd ions and its detrimental effect on cell viability.[58] In the case of MPA-coated heterostructures, there was again very feeble toxicity observed upto the concentration of 1 mg/mL, with cells registering viability above 80 %. This particular observation indicates that in core shell NCs, the metal sulfide shell would have prevented the leaching of Cd ions from the core, thereby relatively improvising the cellular compatibility. Further, PEGylation of the CdSe/Cu_2S was performed utilizing DSPE-PEG-COOH to impart certain additional advantages: (i). to improve the colloidal stability of the NCs, (ii). to reduce oxidation of the NCs, (iii). to improve uptake by cells with augmented biocompatibility and possible escape from serum protein adsorption and RES clearance, among others. [59-61] Apart from the issue of cellular compatibility, it has now become essential to specifically focus the nanomaterials towards malignant cells while evading the normal cells. This has been achieved by grafting various and multiple antibodies, peptides, aptamers etc., on the respective nanomaterial's surface for enhanced recognition and internalization by cancer or related phenotypes alone.[62,63] Folate is well known to facilitate entry of nanoparticles into cancer cell's cytosol by utilizing folate receptors specifically expressed by malignant cell's surface. Folate receptor is the most common type of over-expressed receptor in most cancer types and gliomas are well known to over-express them.[64-67] To this extent, DSPE-PEG-FOL was conjugated onto the CdSe/Cu_2S NCs to render precise and specific cancer cell targeting ability. The conjugation was confirmed

using FT-IR analysis (Fig. 8b) with peaks at 1500 cm^{-1}, arising due to benzene loop backbone stretch of folate and 1686 cm^{-1}, arising due to amide bond formed between folate and PEG moiety. The peaks at 1175 cm^{-1} (C-O-C ether stretch bond), 2918 cm^{-1} (-CH_2 stretching vibrations) and 981 cm^{-1} (-CH out of plane bending vibrations) confirmed the successful grafting of PEG onto the NCs. In addition, zeta potential analysis revealed a negative potential of -41.8 mV, which apart from confirming PEGylation of the NCs, also affirmed their colloidal stability in aqueous neutral pH solution. The observed zeta potential value is ideal for stabilizing conventional aqueous dispersion, as ASTM defines colloids with zeta potentials higher than 40 mV (negative or positive) to have ‘‘good stability’’.[68,69] Post PEGylation, the CdSe-Cu_2S heterostructures presented enhanced cytoamiability even at the concentration of 1 mg/mL (Fig. 8c) post 72 h of incubation. The cellular viability remained above 90 %, on par with the non-NCs treated samples.

The in-cell imaging ability based on the visible luminescence of CdSe in the MPA CdSe, CdSe/Cu_2S and PF-CdSe/Cu_2S NCs were profiled at 561 nm excitation in a CLSM. The NCs were identified by the bright red discrete fluorescence in the cytosol of the cells (Fig. 9c, g, k, o, s, w). The prominent and uniform staining of nucleus by Hoechst (Fig. 9b, f, j, n, r, v), in addition to confirming the lack of any NCs fluorescence in this compartment, also displayed a healthy nuclear staining pattern which was depictive of the non-nuclear toxic nature of the NCs. The luminescence of CdSe as well as core-shell structures were on par with each other under similar exposure time (1 sec), suggesting the utilization of these heterostructures in live cell bioimaging without significantly compromising the fluorescence properties of the core QDs.

Though both CdSe QDs and CdSe/Cu_2S NCs were found to freely enter the cellular compartments of both normal HCN-1A and cancerous Gliomas (Fig. 9c, g, k, o), the PF- CdSe/Cu_2S NCs were seen to gain entry preferentially within 1 h of exposure into cancer cells alone (Fig. 9w). The endocytosis mediated (most common pathway of NPs intake) entry of NCs would need longer times, say 2 h as in the case with the non-targeted NCs whereas, receptor mediated intake requires much lesser time as with the folate-targeted NCs. As normal cells possess threshold level of folate receptor expression, the uptake of particles would be significantly lower than cancer cells that express multitudes of increase in receptor expression allowing for the specific accumulation of NCs and leading to a higher probability of achieving desired effects on malignant cells alone. This preferential uptake of the targeted NCs by cancer cells could be attributed to the over-expressed folate receptors in these cells, which although present in normal cells, but with a drastically reduced number and distribution frequency. ICP-MS analysis supplemented the visual observations, with nearly 35 % of targeted NCs found to gain entry into cancer cells, whereas only 8 % of targeted NCs gained entry into HCN-1A (Tab. 1).

As was previously demonstrated (Fig. S7), the NIR induced thermal responsiveness of the Cu_2S shell in the heterostructures could be further utilized for photothermal therapy (PTT). HCN-1A and Glioma were incubated with either targeted or non-targeted NCs at concentration of 0.1 mg/mL for 2 h, and then exposed to NIR laser irradiation for 4 min. As shown in figure 10a1-a4 and d1-d4, control cells (without NCs) with or without NIR exposure did not show any cell death. Nearly all the cells stained positive to calcein (Fig. 10a2, d2), which is generated by the prominent esterase activity in a live and viable cell and converts Calcein-AM to emit a strong green fluorescence that is indicative of the metabolically active cells. However, when

non-targeted NCs treated HCN-1A and Glioma were irradiated a gradual increase in temperature at the zone of irradiation was observed (Fig. 10b5, e5) which eventually rose to 55 °C and 59 °C, respectively. Post-staining with live/dead dye, both the plates exhibited a necrotic spot (Fig. 10b3, e3), stained positive to propidium iodide, a nuclei staining dye that cannot pass through a viable cell membrane but reaches the nucleus by passing through disordered areas of dead cell membrane, surrounded by viable green calcein fluorescent cells (Fig. 10b4, e4). On the other hand the PF-CdSe/Cu_2S, which selectively gained entry to Glioma, presented a zone of irradiation in this particular cell line alone (Fig. 10f4) with no noticeable rise of temperature in the normal HCN-1A (Fig. 10c5). The temperature at laser focal spot on Glioma cultured plates rose gradually and peaked at 55 °C (Fig. 10f5) leading to the prominent necrotic spot.

Conclusions:

In summary, the results acquired during the course of this study revealed that JC oil could eventually be projected as an alternative industrially relevant solvent. The oil, with its appreciable physico-chemical qualities possesses nearly all the relevant components required for an optimum nanomaterial synthesis medium. As discussed earlier, the utilization of JC oil and the like, lifts the burden off other edible products that are currently being explored for applications as mentioned in this report. The CdSe QDs synthesized from JC oil were of good quality with high colloidal stability and exhibiting significant photoluminescent properties. Also, the coating of these QDs with Cu_2S not only provided a shielding effect to preserve the luminescence and curb toxic aspects of the QDs, but additionally were utilized for PTT. The heterostructure, with its visible and NIR emissions, along with the photo acoustic and

X-ray contrast responsiveness presents an opportunity for employing them as multimodal imaging systems. The specific targeting achieved with folate highly warranted the preferential entry of these NCs into cancerous cells alone with profound photothermal ablation effects. The nanomaterials are projected for their individual and combined properties and their prospects in bioimaging coupled therapeutic strategies. Also, this JC oil based synthesis module could be extended to various other nanomaterial syntheses with multifunctional applications.

Acknowledgements

Part of this study has been supported by a grant for the programme of strategic research foundation at private universities S1101017, organized by the Ministry of Education, Culture, Sports, Science and Technology (MEXT), Japan since April 2012. Imaging studies were in part, supported by a National Institutes of Health Cancer Center Support Grant (P30 CA016672). We thank the Japan Bio-Energy Development Corporation (JBEDC), Japan, for generously providing the seeds of *Jatropha curcas* for this study.

Reference:

[1] Q. Cao , H. S. Kim , N. Pimparkar, J. P. Kulkarni, C. Wang, M. Shim , K. Roy, M. A. Alam, J. A. Rogers, *Nature*, 2008, **454**, 495.
[2] A. Javey, J. Guo, Q. Wang, M. Lundstrom, H. Dai, *Nature*, 2003, **424**, 654.
[3] K. Ryu, A. Badmaev, C. Wang, A. Lin, N. Patil, L. Gomez, A. Kumar, S. Mitra, H. S. P. Wong, C. Zhou, *Nano Lett.*, 2009, **9**, 189.
[4] Y. Lu, J. Liu, *Acc. Chem. Res.*, 2007, **40**, 315.
[5] H. Xing, N. Y. Wong, Y. Xiang, Y. Lu, *Curr. Opin. Chem. Biol.*, 2012, **16**, 429.
[6] N. Y. Wong, H. Xing, L. H. Tan, Y. Lu, *J. Am. Chem. Soc.*, 2013, **135**, 2931.
[7] A. C. Poulose, S. Veeranarayanan, M. S. Mohamed, Y. Nagaoka, R. R. Aburto, T. Mitcham, P. M. Ajayan, R. R. Bouchard, Y. Sakamoto, Y. Yoshida, T. Maekawa, D. S. Kumar, *Nanoscale*, 2015, **7**, 8378.
[8] A. C. Poulose, S. Veeranarayanan, M. S. Mohamed, Y. Sakamoto, N. Hirosawa, Y. Suzuki, M. Zhang, M. Yudasaka, N. Radhakrishnan, T. Maekawa, P. V. Mohanan, D. S. Kumar, *Nanoscale*, 2015, **7**, 13061.
[9] D. A. Tomalia, *Macromol. Symp.*, 1996, **101**, 243.

[10] M. F. Kircher, U. Mahmood, R. S. King, R. Weissleder, L. Josephson, *Cancer Res.*, 2003, **63**, 8122.
[11] K. T. Yong, *Nanotechnology,* 2009, **20**, 015102.
[12] R. Koole, M. M. van Schooneveld, J. Hilhorst, K. Castermans, D. P. Cormode, G. J. Strijkers, C. de Mello Donegá, D. Vanmaekelbergh, A. W. Griffioen, K. Nicolay, Z. A. Fayad, A. Meijerink, W. J. Mulder, *Bioconjug. Chem.*, 2008, **19**, 2471.
[13] N. C. Reichardt, M. Martin-Lomas, S. Penades, *Chem. Soc. Rev.*, 2013, **42**, 4358.
[14] E. Katz, I. Willner, *Angew. Chem. Int. Ed.*, 2004, **43**, 6042.
[15] S. Veeranarayanan, A. C. Poulose, M. S. Mohamed, S. H. Varghese, Y. Nagaoka, Y. Yoshida, T. Maekawa, D. S. Kumar, *Small*, 2012, **8**, 3476.
[16] D-E. Lee, H. Koo, I-C. Sun, J. H. Ryu, K. Kim, I. C. Kwon, *Chem. Soc. Rev.*, 2012, **41**, 2656.
[17] C. Salvador-Morales, P. M. Valencia, A. B. Thakkar, E. W. Swanson, R. Langer, *Front. Biosci.*, 2012, **4**, 529.
[18] X. Hu, X. Hao, Y. Wu, J. Zhang, X. Zhang, P. C. Wang, G. Zou, X-J. Liang, *J. Mater. Chem. B Mater. Biol. Med.*, 2013, **1**, 1109.
[19] K. Kim, J. H. Kim, H. Park, Y-S. Kim, K. Park, H. Nam, S. Lee, J. H. Park, R-W. Park, I-S. Kim, K. Choi, S.Y. Kim, K. Park, I. C. Kwon, *J. Control. Release*, 2010, **146**, 219.
[20] G. Bao, S. Mitragotri, S. Tong, *Annu. Rev. Biomed. Eng*. 2013, **15**, 253.
[21] F. Jia, X. Li, L. Li, S. Mallapragada, B. Narasimhan, Q. Wang, *J. Control. Release*, 2013, **172**, 1020.
[22] M. S. Mohamed, S. Veeranarayanan, A. C. Poulose, Y. Nagaoka, H. Minegishi, Y. Yoshida, T. Maekawa, D. S. Kumar, *Biochim. Biophys. Acta*, 2014, **1840**, 1657.
[23] G. A. Sotiriou, *WIRES Nanomedicine and Nanobiotechnology*, 2013, **5**, 19.
[24] B. Dubertret, M. Calame, A. J. Libchaber, *Nat. Biotechnol.*, 2001, **19**, 365.
[25] T. Pons, I. L. Medintz, K. E. Sapsford, S. Higashiya, A. F. Grimes, D. S. English, H. Mattoussi, *Nano Lett.*, 2007, **7**, 3157.
[26] O. Kulakovich, N. Strekal, A. Yaroshevich, S. Maskevich, S. Gaponenko, I. Nabiev, U. Woggon, M. Artemyev, *Nano Lett.*, 2002, **2**, 1449.
[27] Y. Jin, X. Gao, *Nat. Nanotechnol.*, 2009, **4**, 571.
[28] J. Kasthuri, S. Veerapandian, N. Rajendiran, *Colloids Surf. B*, 2009, **68**, 55.
[29] A. R. V. Nestor, V. S. Mendieta, M. A. C. Lopez, R. M. G. Espinosa, M. A. C. Lopez, J. A. A. Alatorre, *Mater. Lett.*, 2008, **62**, 3103.
[30] S. P. Chandran, M. Chaudhary, R. Pasricha, A. Ahmad, M. Sastry, *Biotechnol. Prog.*, 2006, **22**, 577.
[31] H. Kamiya, M. Iijima, *Sci. Technol. Adv. Mater.*, 2010, **11**, 044304.
[32] M. J. Mulvihill, S. E. Habas, H. Jen-La Plante, J. Wan, T. Mokari, *Chem. Mater.*, 2010, **22**, 5251.
[33] M. Green, *J. Mater. Chem.*, 2010, **20**, 5797.
[34] N. Pradhan, D. D. Reifsnyder, R. R. Xie, J. J. Aldana, X. X. Peng, *J. Am. Chem. Soc*., 2007, **129**, 9500.
[35] N. Pradhan, D. M. Battaglia, Y. Liu, X. Peng, *Nano Lett.*, 2007, **7**, 312.
[36] A. Dong, F. Wang, T. L. Daulton, W. E. Buhro, *Nano Lett.*, 2007, **7**, 1308.
[37] S. A. Santangelo, E. A. Hinds, V. A. Vlaskin, P. I. Archer, D. R. Gamelin, *J. Am. Chem. Soc.*, 2007, **129**, 3973.

[38] N. R. Xiao, Q. Q. Dai, Y. N. Wang, J. J. Ning, B. B. Liu, G. T. Zou, B. Zou, *J. Hazard. Mater.*, 2012, **211**, 62.
[39] P. Zhang, Y. Sui, C. Wang, Y. Wang, G. Cui, C. Wang, B. Liu, B. Zou, *Nanoscale*, 2014, **6**, 5343.
[40] S. Sapra, A. L. Rogach, J. Feldmann, *J. Mater. Chem.*, 2006, **16**, 3391.
[41] M. Debnath, P. S. Bisen, *Curr. Pharm. Biotechnol.*, 2008, **9**, 288.
[42] B. N. Divakara, H. D. Upadhyaya, S. P. Wani, C. L. L. Gowda, *Appl. Energy*, 2010, **87**, 732.
[43] A. J. King, W. He, J. A. Cuevas, M. Freudenberger, D. Ramiaramanana, I. Graham, *J. Exp. Bot.*, 2009, **60**, 2897.
[44] R. E. E. Jongschaap, W. J. Corre, P. S. Bindraban, W. A. Brandenburg, *Plant Research International*, Wageningen UR, The Netherlands 2007, Report 158.
[45] C. Baroi, E. K. Yanful, M. A. Bergougnou, *Int. J. Chemical Reactor Engineering*, 2009, **7,** 1542.
[46] Z. Yin, Y. Zhang, K. Chen, J. Li, W. Li, P. Tang, H. Zhao, Q. Zhu, X. Bao, D. Ma, *Sci. Rep.*, 2014, **4**, 4288.
[47] C. de. M. Donega, *Chem. Soc. Rev.*, 2011, **40**, 1512.
[48] B. Fritzinger, I. Moreels, P. Lommens, R. Koole, Z. Hens and J. C. Martins, *J. Am. Chem. Soc.*, 2009, **131**, 3024.
[49] A. Hassinen, I. Moreels, C. de Mello Donega, J. C. Martins, Z. Hens, *J. Phys. Chem. Lett.*, 2010, **1**, 2577.
[50] S. D. B. Kouame, J. Perez, S. Eser, A. Benesi, *Fuel Processing Technology*, 2012, **97**, 60.
[51] C. Fauhl, F. Reniero, C. Guillou, *Magn. Reson. Chem.*, 2000, **38**, 436.
[52] J. Salimon, B. M. Abdullah, N. Salih, *Chemistry Central Journal*, 2011, **5**, 67.
[53] Q. Li, S. Guo, P. Xu, L. Wu *Cryst. Res. Technol.*, 2013, **48**, 977.
[54] Y. Xie, A. Riedinger, M. Prato, A. Casu, A. Genovese, P. Guardia, S. Sottini, C. Sangregorio, K. Miszta, S. Ghosh, T. Pellegrino, L. Manna, *J. Am. Chem. Soc.*, 2013, **135**, 17630.
[55] Q. Tian, F. Jiang, R. Zou, Q. Liu, Z. Chen, M. Zhu, S. Yang, J. Wang, J. Wang, J. Hu, *ACS Nano*, 2011, **5**, 9761.
[56] B. Li, Q. Wang, R. Zou, X. Liu, K. Xu, W. Li, J. Hu, *Nanoscale*, 2014, **6**, 3274.
[57] D. K. Roper, W. Ahn, M. Hoenfner, *J. Phys. Chem.*, *C* 2007, **111**, 3636.
[58] S. Veeranarayanan, A. C. Poulose, M. S. Muhamed, Y. Nagaoka, S. Iwai, Y. Nakagame, S. Kashiwada, Y. Yoshida, T. Maekawa, D. S. Kumar, *Int. J. Nanomed.*, 2012, **7**, 3769.
[59] J. Suh, K. L. Choy, S. K. Lai, J. S. Suk, B. C. Tang, S. Prabhu, J. Hanes, *Int. J Nanomed.*, 2007, **2**, 735.
[60] J. V. Jokerst, T. Lobovkina, R. N. Zare, S. S. Gambhir, *Nanomedicine*, 2011, **6**, 715.
[61] H. Otsuka, Y. Nagasaki, K. Kataoka, *Adv. Drug Deliv. Rev.*, 2003, **55**, 403.
[62] A. D. Friedman, S. E. Claypool, R. Liu, *Curr. Pharm. Res.*, 2013, **19**, 6315.
[63] Z. Xiao, E. L. Nissenbaum, F. Alexis, A. Lupták, B. A. Teply, J. M. Chan, J. Shi, E. Digga, J. Cheng, R. Langer, O. C. Farokhzad, *ACS Nano*, 2012, **6**, 696.
[64] S. A. Kularatne, P. S. Low, *Methods Mol. Biol.*, 2010, **624**, 249.

[65] X. Wang, J. Li, Y. Wang, L. Koenig, A. Gjyrezi, P. Giannakakou, E. H. Shin, M. Tighiouart, Z. G. Chen, S. Nie, D. M. Shin, *ACS Nano*, 2011, **5**, 6184.
[66] N. Parker, M. J. Turk, E. Westrick, J. D. Lewis, P. S. Low, C. P. Leamon, *Anal. Biochem.*, 2005, **338**, 284.
[67] H. S. Yoo, T. G. Park, *J Control. Rel.*, 2004, **100**, 247.
[68] Y. C. Si, E. T. Samulski, *Nano Lett.*, 2008, **8**, 1679.
[69] Y. Shen, L. Li, Q. Lu, J. Ji, R. Fei, J. Zhang, E. S. Abdel-Halim, J-.J. Zhu, *Chem. Commun.*, 2012, **48**, 2222.

FIGURES & TABLE

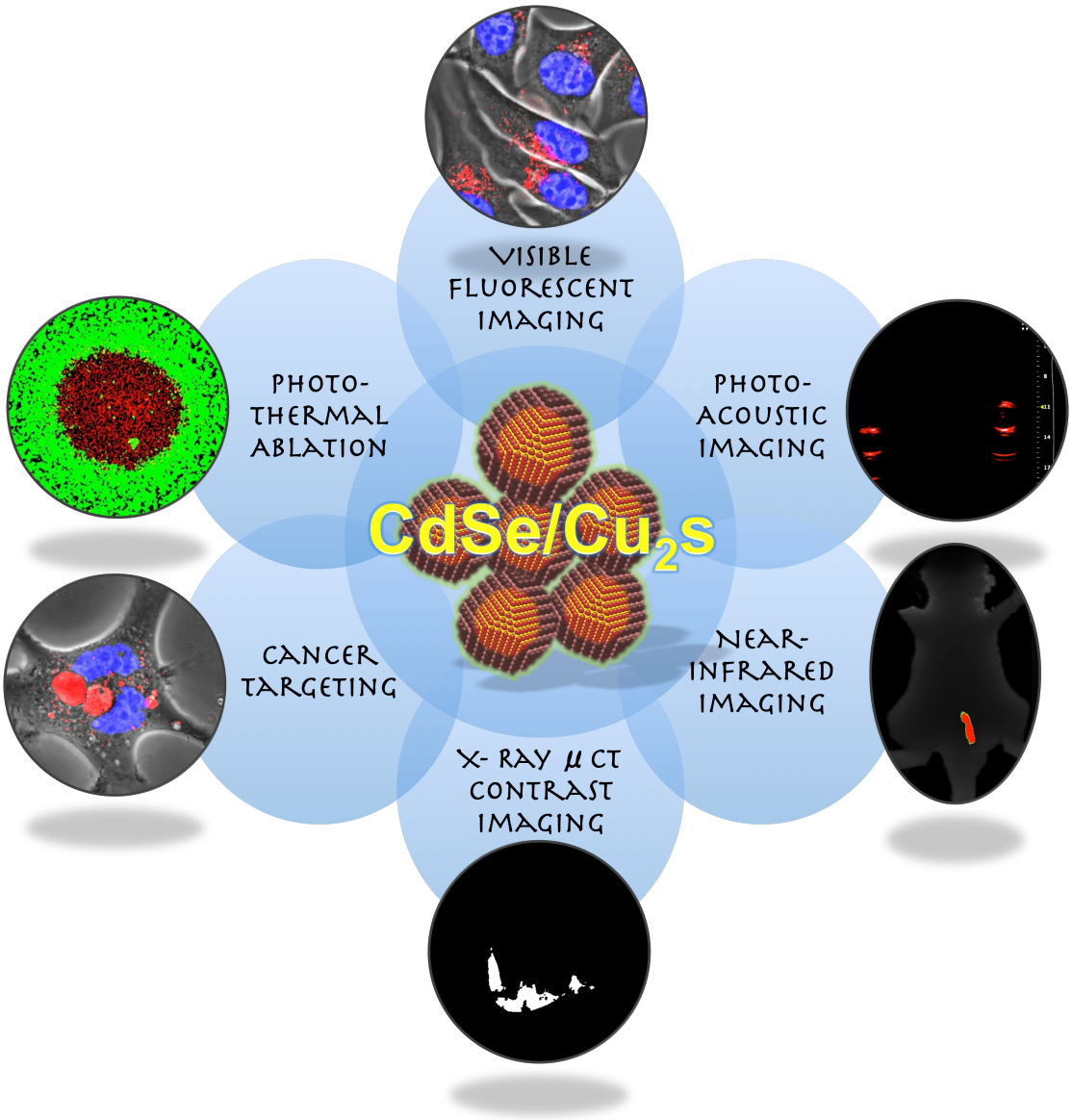

TOC: The applications of CdSe/Cu_2S hybrid nanocrystals in multimodal bioimaging and photo thermal therapy.

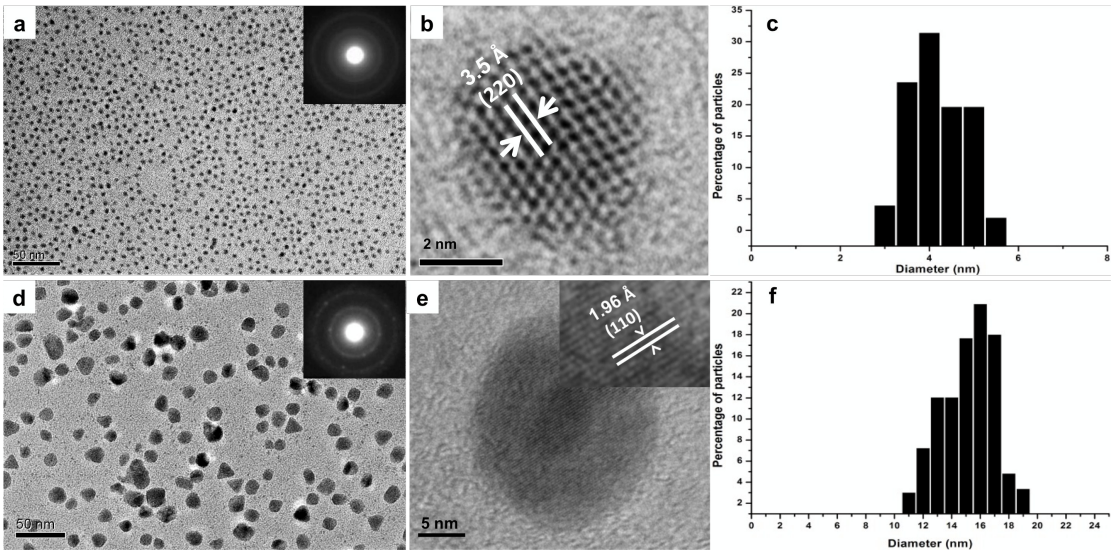

Fig. 1. TEM micrographs of the CdSe QDs (a). The QDs were highly monodisperse with high degree of self-assembly. The crystal lattice arrangement could be clearly observed from the HRTEM image (b) and corresponding SAED pattern (inset). (c) The size distribution plot reveals particle size of 3-5 nm. The CdSe/Cu_2S NCs were seen to be relatively monodisperse with minimum aggregation (d) and size of 13-17 nm (f). The HRTEM (e) clearly demarcates the core CdSe from the Cu_2S shell.

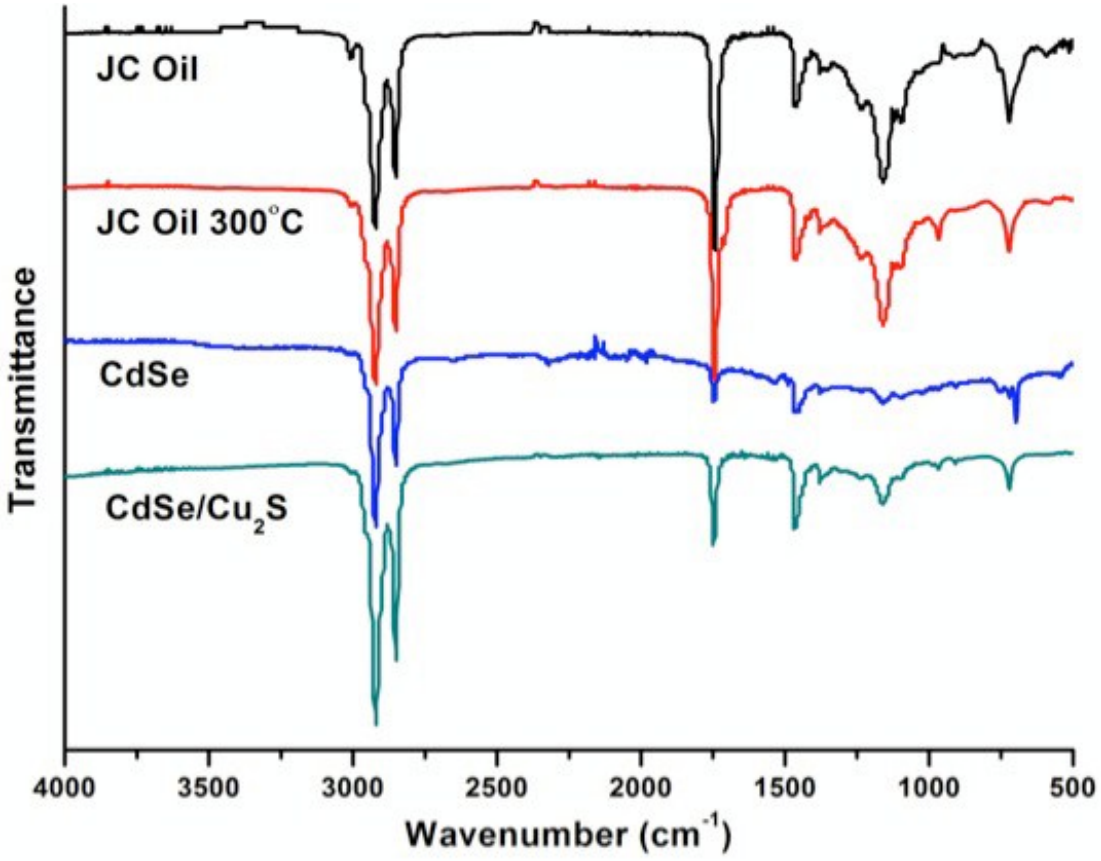

Fig. 2. The FT-IR spectrum of the oil and NCs reveals similar peaks with variation in their intensities. The presence of all characteristic peaks of native oil in the 300 °C treated oil suggests the robustness of the oil to withstand high temperatures without denaturation. Similar peaks were observed in the case of the CdSe QDs and the CdSe/Cu_2S NCs which preferentially arise due to the capping of the NCs by oil fatty acid ligands during synthesis.

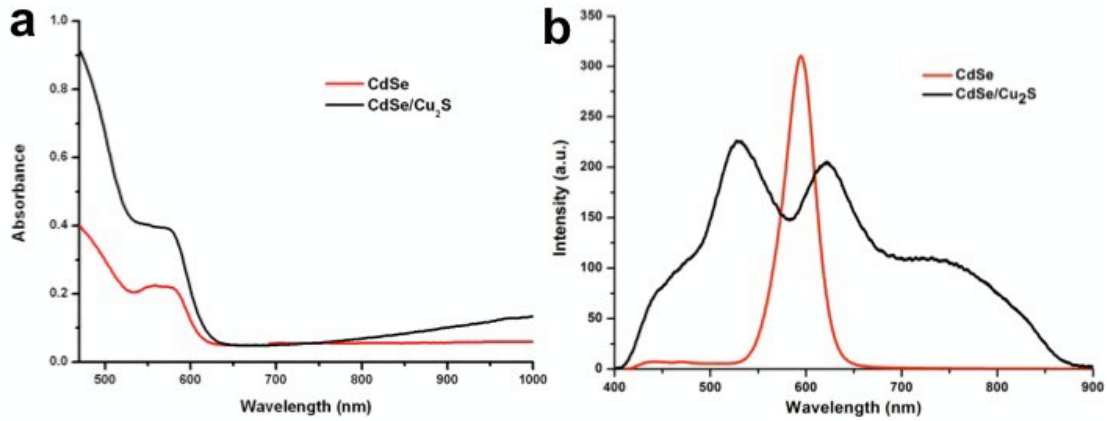

Fig. 3. The UV/Vis spectra of CdSe and CdSe/Cu_2S NCs (a) present peaks centered at 570 nm and a broad region in the case of the latter in the NIR zone. The CdSe QDs exhibited a sharp peak at 590 nm in the photoluminescence spectra (b) whereas the CdSe/Cu_2S NCs presented multiple discrete peak regions at 520 and 625 nm and a shoulder peak in the NIR region.

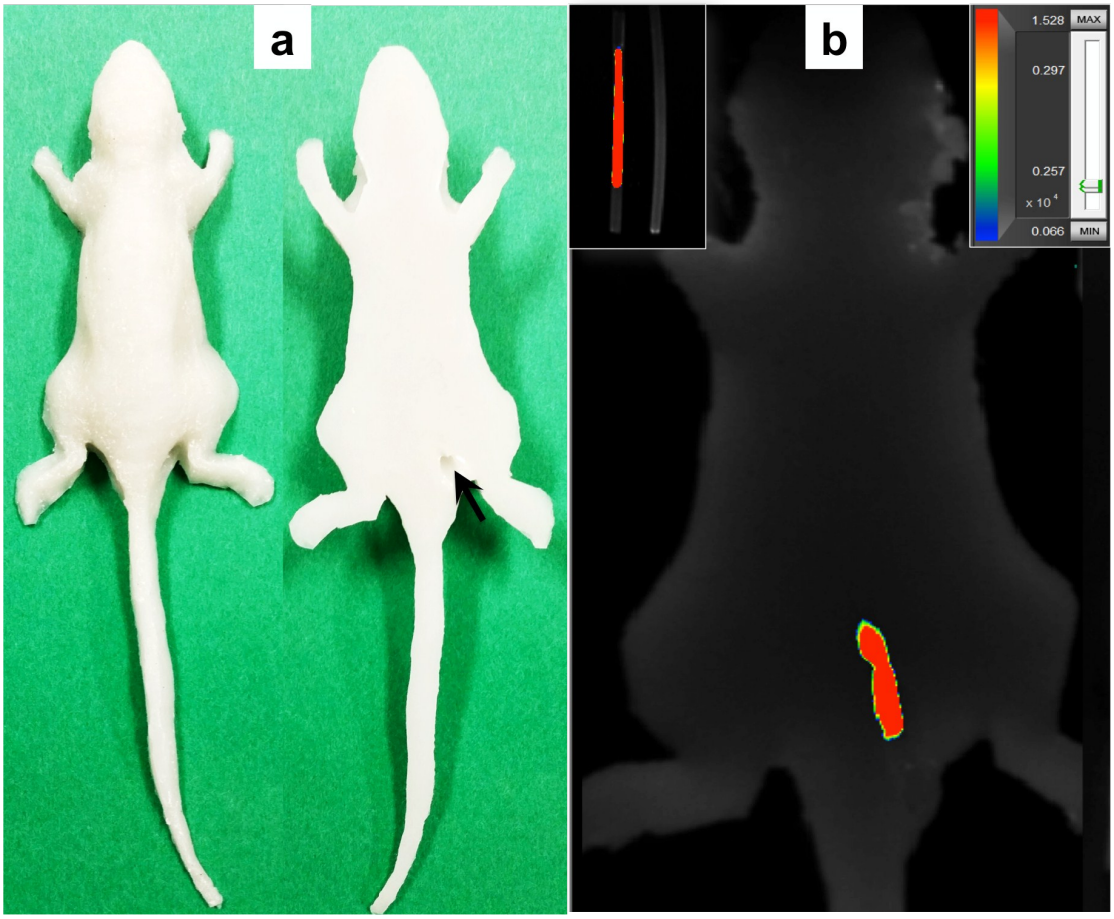

Fig. 4. NIR based optical imaging of NCs using mice phantoms under Cy 7 filter with an excitation wavelength, 650 nm and emission at 810 nm. a) Photographs of dorsal and ventral view of in-house built mouse phantom. (a). PDMS based mouse phantoms. The right panel shows the diagonal orifice (black arrow) into which the NCs filled tube was inserted. b) The NCs filled silicon tubing presented marked fluorescence under Cy 7 excitation and there was no interference from the tube itself (left inset). On insertion of the tube inside the mouse phantom, bright fluorescence was observed from the tube spanning the entire thickness of the phantom.

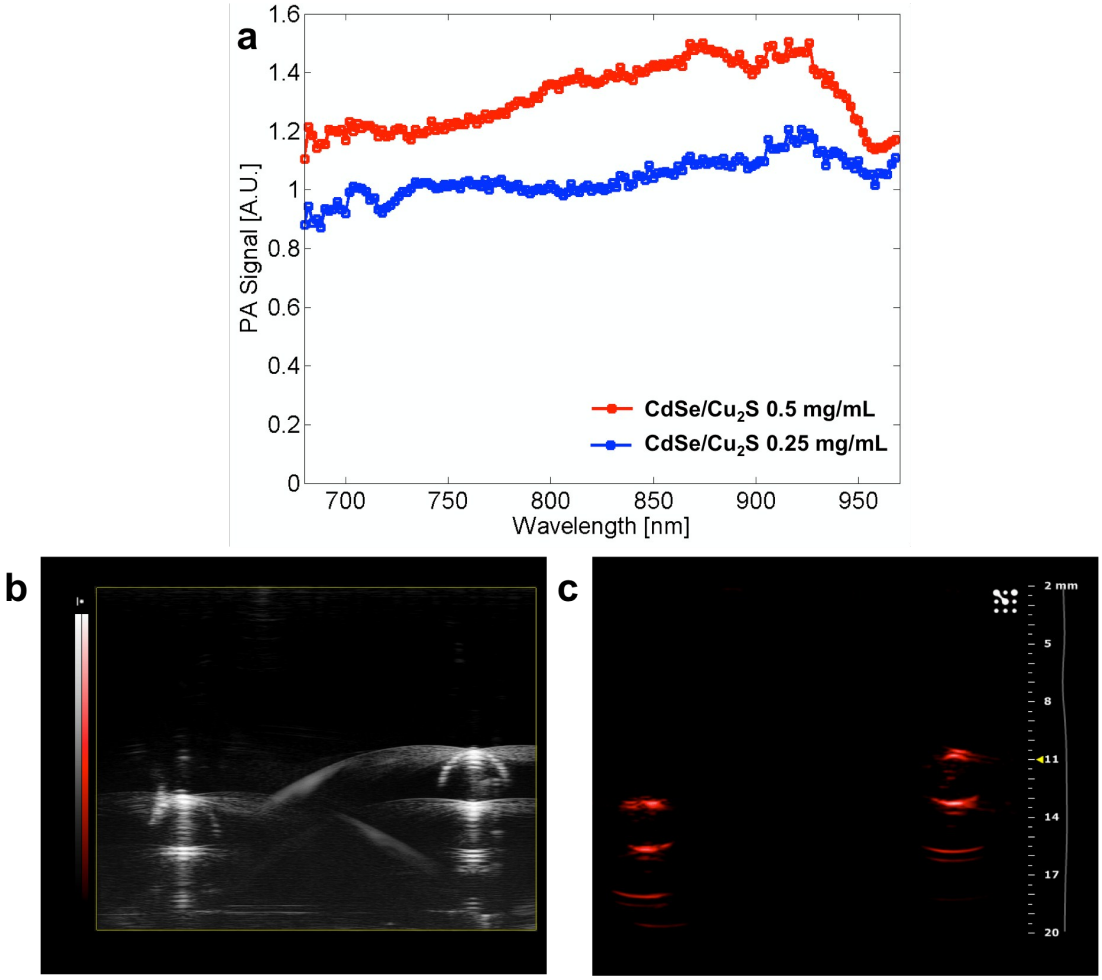

Fig. 5. Photoacoustic imaging (a). Normalized photoacoustic signal spectrum of PEGylated CdSe/Cu_2S NCs (b). Ultrasound B-mode image and (c). Photoacoustic image of NCs filled vinyl tube phantom.

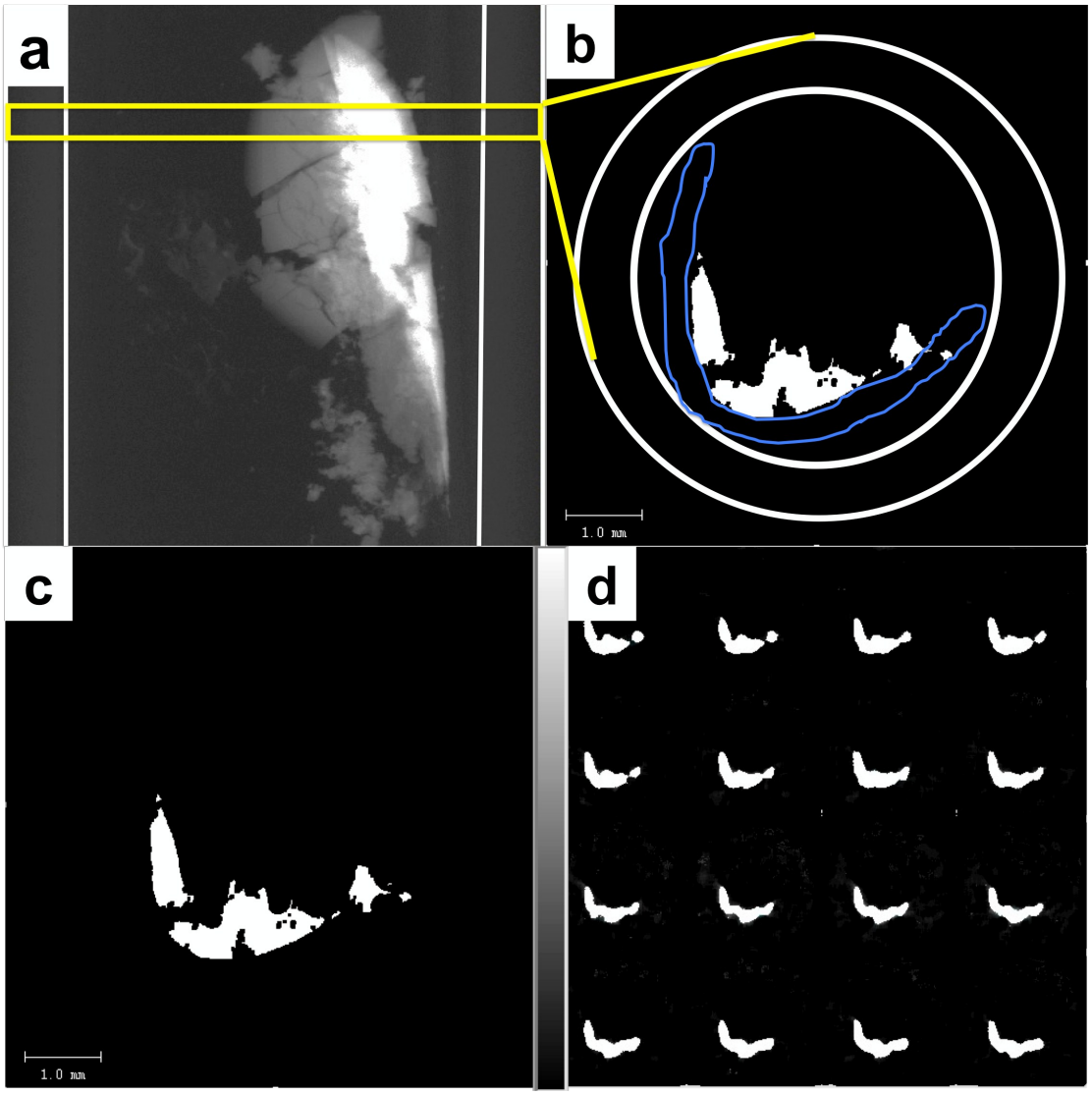

Fig. 6. X-Ray μ CT contrast imaging of CdSe/Cu_2S NCs. (a). Scout view (lateral) of sample on a filter paper strip. The region marked with yellow boundary was further investigated for contrast acquisitions. (b). The blue boundary depicts the filter paper strip inside the holder phantom (white circles). The high contrast from the sample could be visualized with negative interference from the paper strip. (c). Z-stacked contrast image of the multi-CT slices (d) of the selected region.

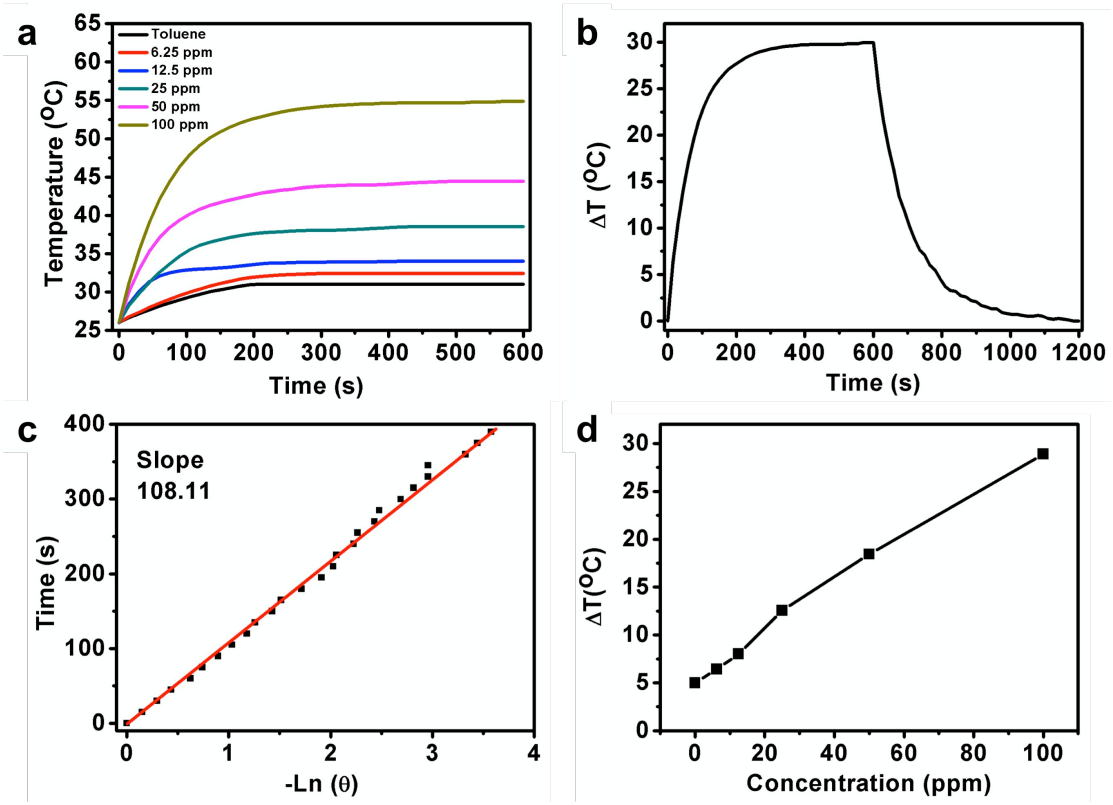

Figure 7: Photothermal Efficacy of CdSe/Cu_2S NCs. a) Heating profile of different concentrations (1, 10, 30, 50, 100 ppm) of PEG-Cu_2S NCs (suspended in water) upon NIR irradiation. b) Plot of difference in temperature attained upon 600 sec (10 min) NIR irradiation of different concentrations of PEG-Cu_2S NCs. c) The heating and cooling profile of 100 ppm PEG-Cu_2S NCs in terms of difference in temperature. The sample was irradiated for 600 sec, post that the laser is shut down and the gradual drop in temperature was recorded until the temperature attains initial room temperature. d) Plot of cooling period (after 600 s) versus negative natural logarithm of driving force temperature. Time constant (τs) for heat transfer is determined to be 133.20 s.

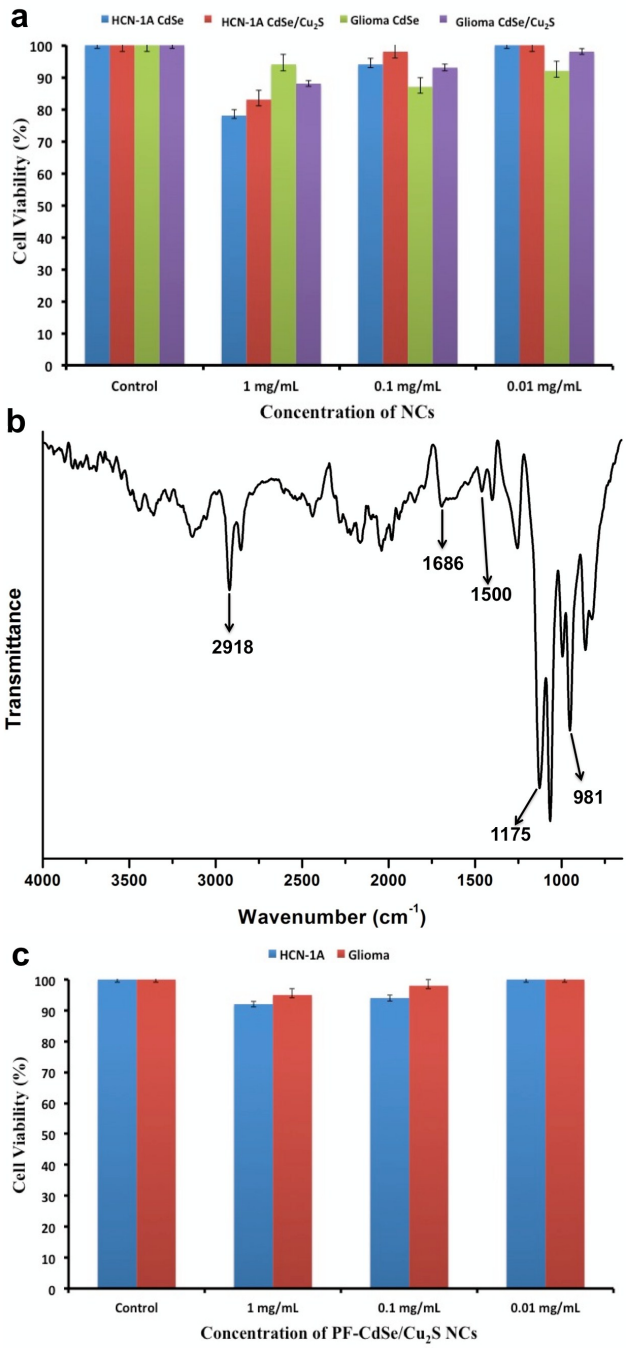

Fig. 8. The cytocompatibility of MPA coated nanomaterials was tested on the HCN-1A and Glioma cells (a). Both of the NCs did not present any significant detrimental effects on the cellular viability even at high concentrations. The PEGylation of the CdSe/Cu_2S NCs was confirmed by the presence of characteristic peaks of folate at 1500 cm^{-1} and PEG-folate amide bond at 1686 cm^{-1} respectively (b). The cytocompatibility of the PF- CdSe/Cu_2S NCs was tested to assess the effectiveness of PEGylation (c). The nanomaterial did not show any toxicity to the cells with both cell lines registering viability above 90 %.

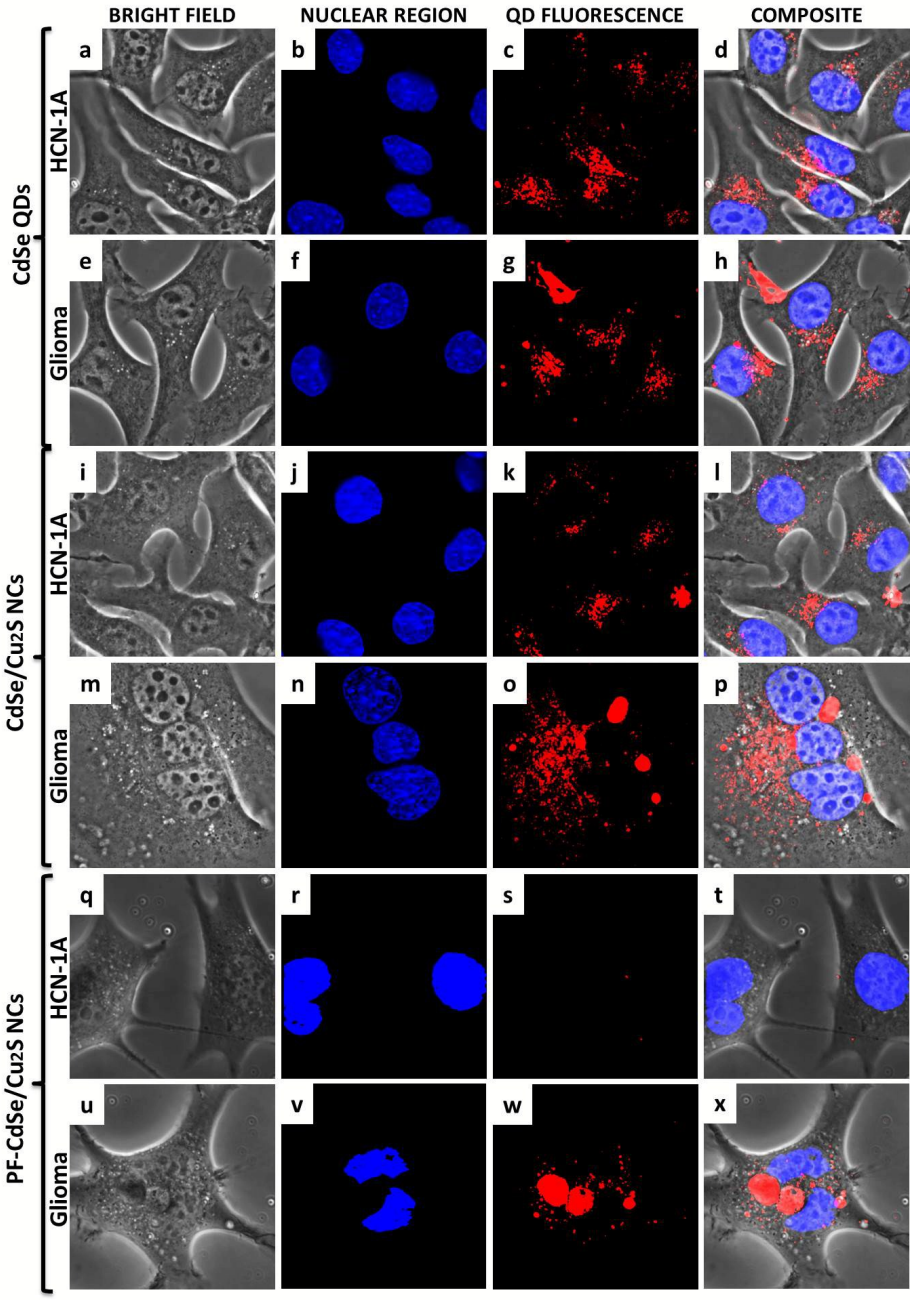

Fig. 9. The cellular imaging ability of the QDs and core-shell NCs was investigated on live cells. The bare MPA CdSe QDs and CdSe/Cu_2S NCs presented excellent uptake by both normal (c, k) and Glioma (g, o) cells which was evidenced by the discrete red fluorescence form the cytosol of the cells. Most of the particle accumulation was observed to be surrounding the nucleus. In the case of the folate targeted PF- CdSe/Cu_2S NCs the uptake was preferentially limited to the Glioma cells (w) with extremely feeble fluorescence detected for the normal HCN-1A (s), depicting the proper targeting achieved.

Cells	Cu (%)	Cd (%)	Se (%)
HCN-1A – $CdSe/Cu_2S$	37.7	38	34
Glioma - $CdSe/Cu_2S$	32.5	34	29.7
HCN-1A – PF- $CdSe/Cu_2S$	8.2	7.7	8.5
Glioma - PF- $CdSe/Cu_2S$	34.6	39	34

Tab. 1. ICP-MS analysis of NCs entry into normal and cancer cells. The data reveals the significant presence of non-targeted NCs in both glioma and HCN-1A in relatively equal quantity. However, only one-fourth of the PF-$CdSe/Cu_2S$ NCs NCs gained entry into normal cells when compared to those in the cancer cells. Though this data relates to the elemental quantification, the observations support the claim of targeting efficiency of the NCs.

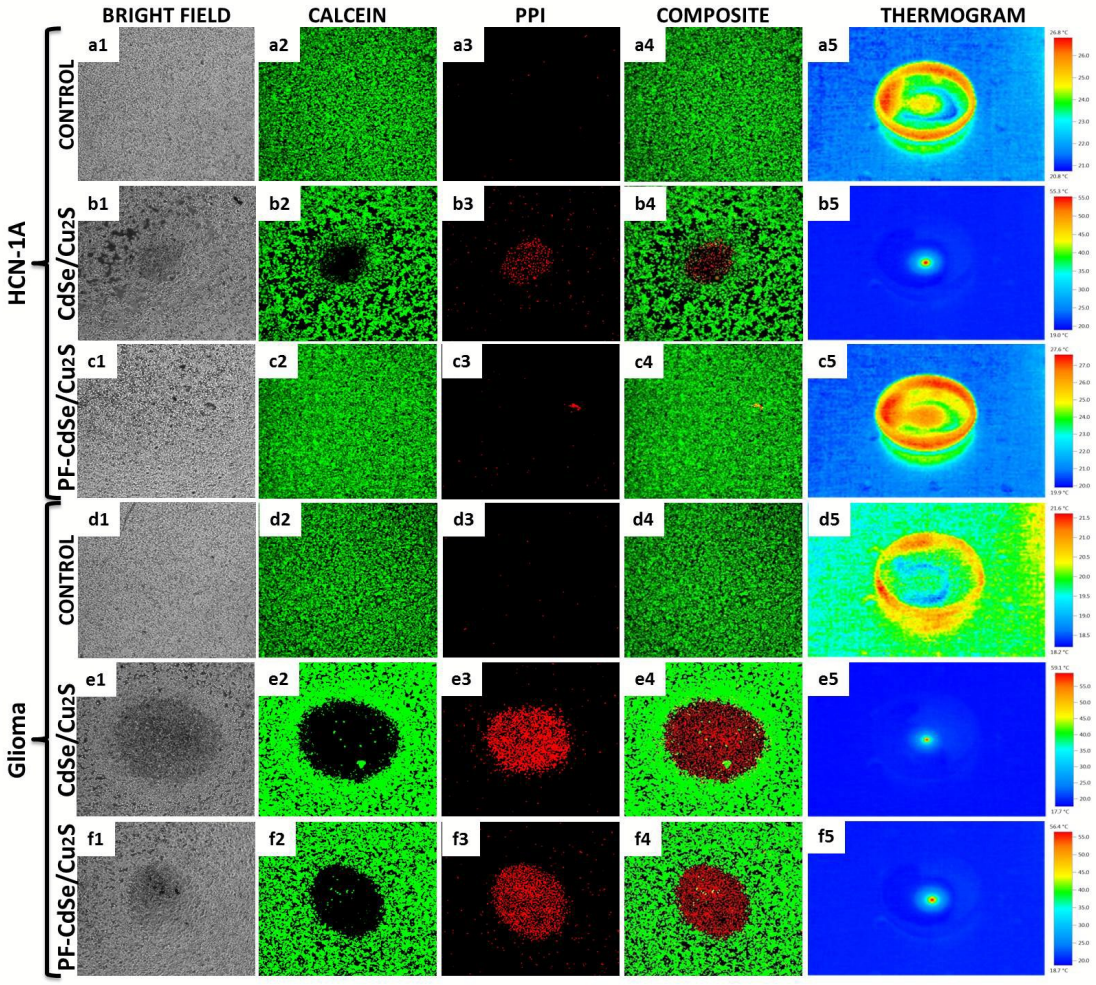

Fig. 10. The photothermal competence of the CdSe/Cu_2S NCs was tested on the cell lines with irradiation by an NIR laser beam. The non-targeted MPA CdSe/Cu_2S NCs presented a significant temperature rise in the case of both normal (b5) and Glioma (e5) cell lines with distinct zones of irradiation, where the laser was incident, demarcating the live cells from the dead (b4, e4). In the case of PF- CdSe/Cu_2S NCs there was a prominent dead zone of cells in the Glioma (f3) cultures with a temperature rise of nearly 56 °C, whereas minimal dead cells were seen in the HCN-1A (c3).